Chapter 8
The Development of New Spirooxindoles Targeting the p53–MDM2 Protein-Protein Interactions for Cancer Therapy

Bin Yu and Hong-Min Liu

8.1 Significance and Structures of p53–MDM2 Interactions

8.1.1 Biological Roles of p53

The TP53 gene-encoded p53 tumor suppressor protein is a transcriptional factor, which plays pivotal roles in regulating cellular processes and suppressing tumor development [1]. In cells, p53 and MDM2 (also known as HDM2 in humans) are tightly regulated through the auto-regulatory negative feedback loop, thus maintaining normal physiological functions (Fig. 8.1) [2, 3]. This auto-regulatory feedback loop operates from the transcription of MDM2 initiated by the p53 activation, leading to the increase in MDM2 mRNA and protein expression. In unstressed cells, because of the low cellular levels and the MDM2-mediated degradation (leading to instability of p53, $T_{1/2} < 30$ min), the growth-suppressing activity of p53 is inhibited [4]. By contrast, the rapid stabilization and expression of p53 induced by cellular stress such as DNA damage, oncogenic activation, hypoxia prevent unwanted propagation and kill defective cells via a dual transcription-dependent/-independent function [5]. However, almost 50% of human cancers fail to express p53 protein as a consequence of the mutation or deletion of TP53 gene

B. Yu · H.-M. Liu (✉)
Ministry of Education, Key Laboratory of Advanced Drug Preparation Technologies, Zhengzhou University, 100 Kexue Avenue, Zhengzhou 450001, Henan, China
e-mail: liuhm@zzu.edu.cn

B. Yu
e-mail: zzuyubin@hotmail.com

B. Yu · H.-M. Liu
Co-innovation Center of Henan Province for New Drug Research & Development and Preclinical Safety, School of Pharmaceutical Sciences, Zhengzhou University, 100 Kexue Avenue, Zhengzhou 450001, Henan, China

C. Sheng and G. I. Georg (eds.), *Targeting Protein-Protein Interactions by Small Molecules*, https://doi.org/10.1007/978-981-13-0773-7_8

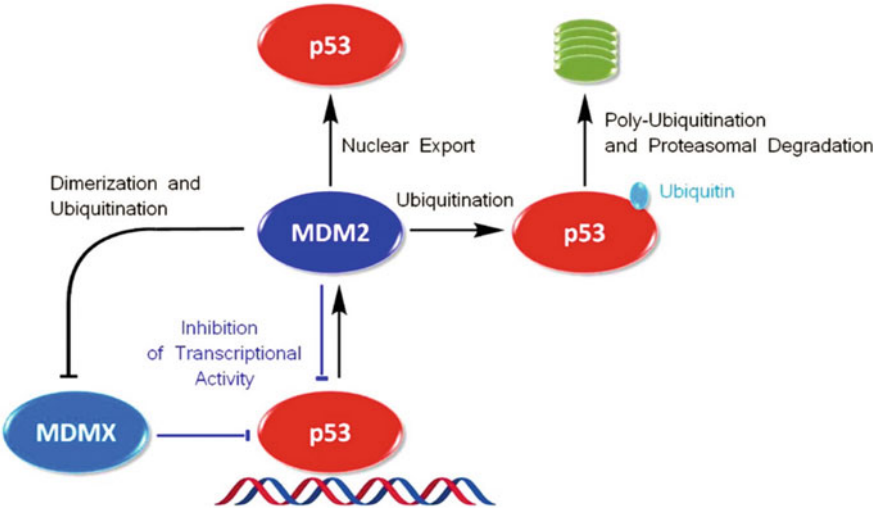

Fig. 8.1 Auto-regulatory feedback loop between p53 and MDM2. Reprinted with permission from Ref. [13]. Copyright © 2014, American Chemical Society

[6]. For those tumors expressing wild-type (wt) p53, their p53 functions are always inhibited through multiple different mechanisms [7–10]: (1) MDM2, as an E3 ubiquitin ligase, promotes ubiquitin-dependent p53 degradation on nuclear and cytoplasmic 26S proteasomes; (2) MDM2 promotes the nuclear export of p53 into the cytoplasm, thereby reducing its transcriptional ability; (3) The binding ability of p53 to its targeted DNA is attenuated by the MDM2–p53 interaction, rendering p53 non-functional [11]. Besides, MDM2 can also bind to p53 directly and inhibits p53 function without leading to p53 degradation. Tumor suppressor ARF stabilizes p53 by binding to MDM2 and sequestering MDM2 into the nucleolus. MDMX, as a regulator of MDM2, inhibits degradation of MDM2 through their interactions at the *C*-terminal RING finger domains [12].

8.1.2 Structures of p53–MDM2 Interactions

In structure, the functional p53 is a homo-tetramer, in which each monomer contains the *N*-terminal transactivation domain, proline-rich domain, sequence-specific DNA-binding domain, and oligomerization domain (Fig. 8.2a), while the MDM2 protein consists of an *N*-terminal p53 interaction domain, a central acidic domain, a zinc-finger domain, and a *C*-terminal RING domain (Fig. 8.2b) [14]. The *N*-terminal transactivation domain in p53 shows a stable helical conformation, where the π–π interaction between Phe19 and Trp23 has proven to be crucial in maintaining its structural stability and functional roles (Fig. 8.2c) [15]. Historically,

the protein-protein interactions (PPIs) have long been recognized as undruggable targets because PPIs usually involve large and flat interfaces that are difficult to break by small molecules [16, 17]. Differently, the co-crystal structure of MDM2–p53 complex in 1996 shows that the interactions between MDM2 and p53 are primarily mediated by a small range of amino acid residues (namely the first ~120 *N*-terminal amino acid residues of MDM2 and the first 30 *N*-terminal residues of p53 [13]) and the MDM2-bound p53 peptide adopts a α-helical conformation and interacts with MDM2 primarily through the Phe19, Trp23, and Leu23 residues, which are inserted into the well-defined hydrophobic cleft in MDM2 (Fig. 8.2d) [13, 18]. The structural features of MDM2–p53 complex provide a basis for designing small molecules that mimic the key residues to block the MDM2–p53 interactions [19]. Substantial efforts have been devoted to developing small molecules and peptides that can disrupt the MDM2–p53 interactions, making p53 a potential target for cancer therapy [11, 20–29].

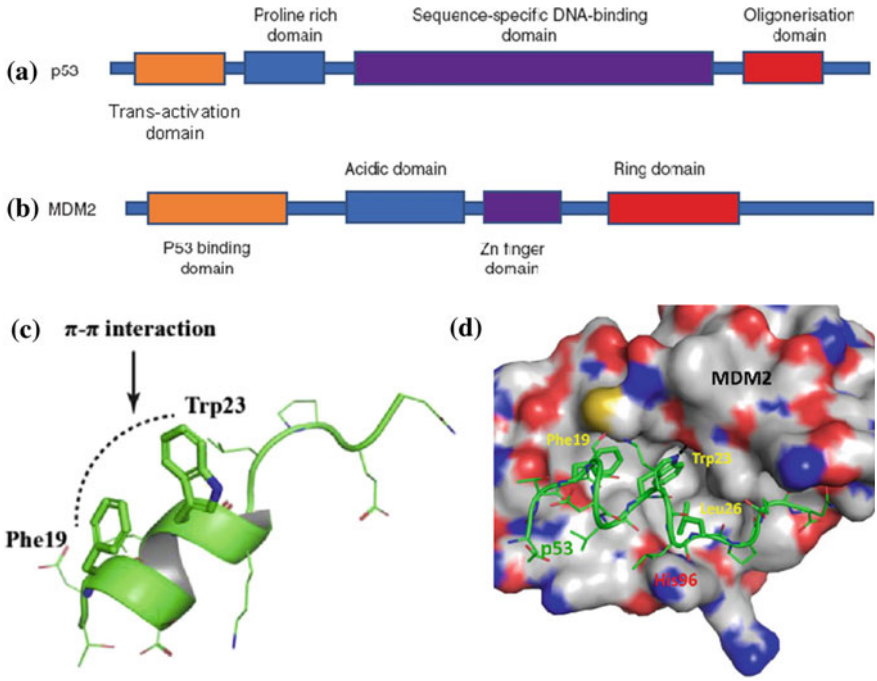

Fig. 8.2 **a**, **b** Major functional domains of p53 and MDM2 proteins, respectively; **c** The *N*-terminal domain of p53; **d** The co-crystal structure of MDM2–p53 complex (PDB code: 1YCR). **a** and **b** were reprinted with permission from Ref. [14]. Copyright © 2010, Elsevier Ltd; **c** was reprinted with permission from Ref. [15]. Copyright © 2015, Elsevier Ltd; **d** was reprinted with permission from Ref. [13]. Copyright © 2014, American Chemical Society

8.1.3 *Small Molecules in Clinical Trials Targeting p53–MDM2 Interactions*

To date, a large number of small-molecule inhibitors targeting the MDM2–p53 interactions have been identified, and these inhibitors can be divided into several chemotypes including imidazolines (e.g., Nutlin series [30], RG-7112), benzodiazepinediones (e.g., TDP665759 [31]), spirooxindoles (e.g., SAR405838 [32, 33]), piperidinones (e.g., AMG232 [34–36] and CGM097 [37]), isoindolinones. Some of them have advanced into clinical trials for anticancer assessment [13], such as SAR405838 [32, 33], MK-8242, DS-3032b, NVP-CGM097 [37–39], RG7112, [40, 41] RG7388, [42] AMG 232 [34–36], and APG-115 [43] (Fig. 8.3). Among them, the structures of MK-8242 and DS-3032b are not available to date.

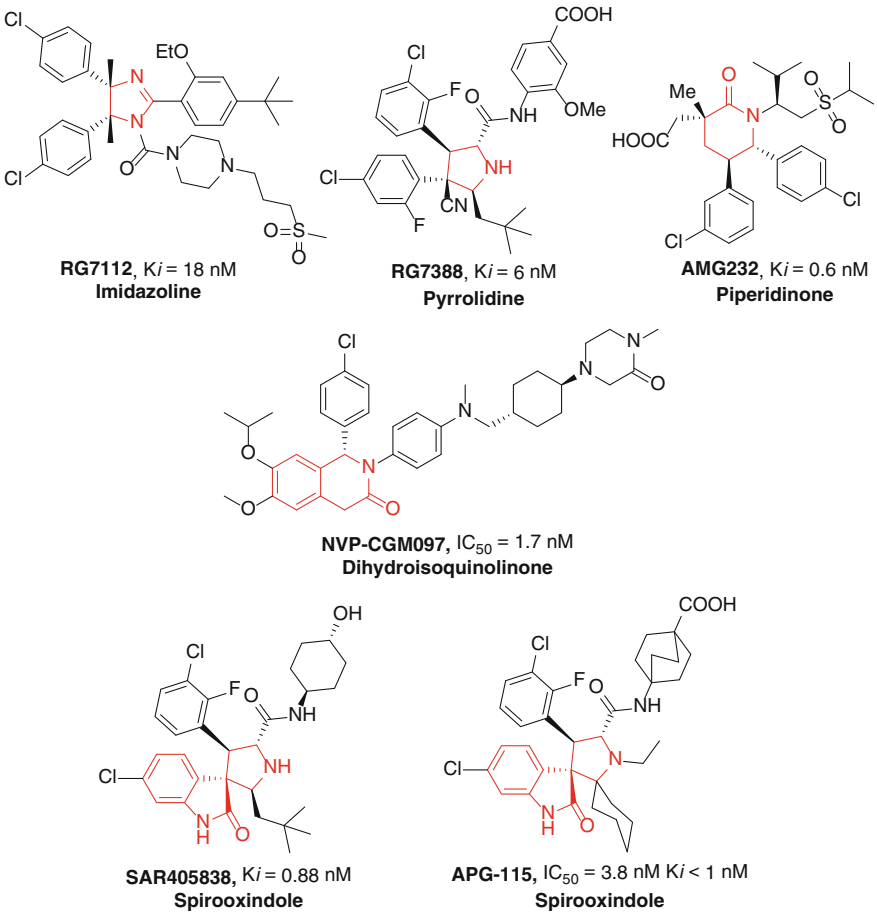

Fig. 8.3 Small-molecule MDM2 inhibitors in clinical trials

In this chapter, we highlight the identification of spirooxindole containing small-molecule inhibitors, strategies employed for optimizations, structure–activity relationship studies (SARs) as well as preclinical data of those undergoing clinical assessment. Based on the SARs and the co-crystal structures of p53–MDM2 complexes, we first propose the prolinamide-based '3+1' model that may be utilized for designing potent MDM2 inhibitors.

8.2 The Development of Spirooxindoles as MDM2–p53 Protein-Protein Interaction Inhibitors

8.2.1 Structure-Based Design and Optimization of Spirooxindoles Targeting MDM2–p53 Interactions

Spirooxindole fragments have recently drawn extensive attention because of their prevalence in natural products (e.g., spirotryprostatin A and B) [44] and biologically active agents (e.g., CFI-400945 [45], KAE609 [46–49], and SAR405838) and have been proved to possess diverse biological activities [45, 50–57]. The structural characteristics of spirooxindoles lie in their spiro scaffolds with other heterocyclic moieties fused at the C3 position of oxindole core. The 3D structural features of spirocycles make spirooxindole scaffolds promising as templates in drug discovery programs, as observed in identifying potent and selective MDM2 inhibitors.

As shown in Fig. 8.2d, the hydrophobic cleft on the surface of MDM2 is occupied by Phe19, Trp23, and Leu26 residues of p53 in a compact and well-defined fashion. Of these three residues, Trp23 is deeply buried inside the narrow and deep hydrophobic cavity in MDM2 and the NH unit of Trp23 residue forms an additional hydrogen bond with the carbonyl group of MDM2. A pioneering work in designing MDM2 inhibitors was carried out by the Wang group, generating a library of potent MDM2 inhibitors, such as the anticancer drug candidate SAR405838 (K_i = 0.88 nM) and the second-generation inhibitor MI-1061 (K_i = 0.16 nM) (Fig. 8.4) [58]. Initially, they found that the oxindole group can closely mimic the Trp23 residue of p53 to occupy the hydrophobic pocket in MDM2, where the amide NH in place of NH in Trp23 served as the hydrogen bond donor [59]. The spiropyrrolidinyl oxindole core (highlighted in Red in Fig. 8.4) was then used as substructure for designing MDM2 inhibitors; another two hydrophobic groups around the pyrrolidinyl ring were projected in a certain manner to mimic Phe19 and Leu26 because of the spatial repulsion of adjacent hydrophobic groups.

Based on the spiropyrrolidinyl oxindole-based substructure, compound **1** (MI-5, K_i= 8.46 μM) was designed to mimic three key residues in p53, but was less potent than natural p53 peptide (K_i = 1.52 μM). Docking studies showed that the phenyl and isopropyl groups of compound **1** mimicked the Phe19 and Leu26 in p53, respectively, to occupy two hydrophobic pockets in MDM2, while the oxindole

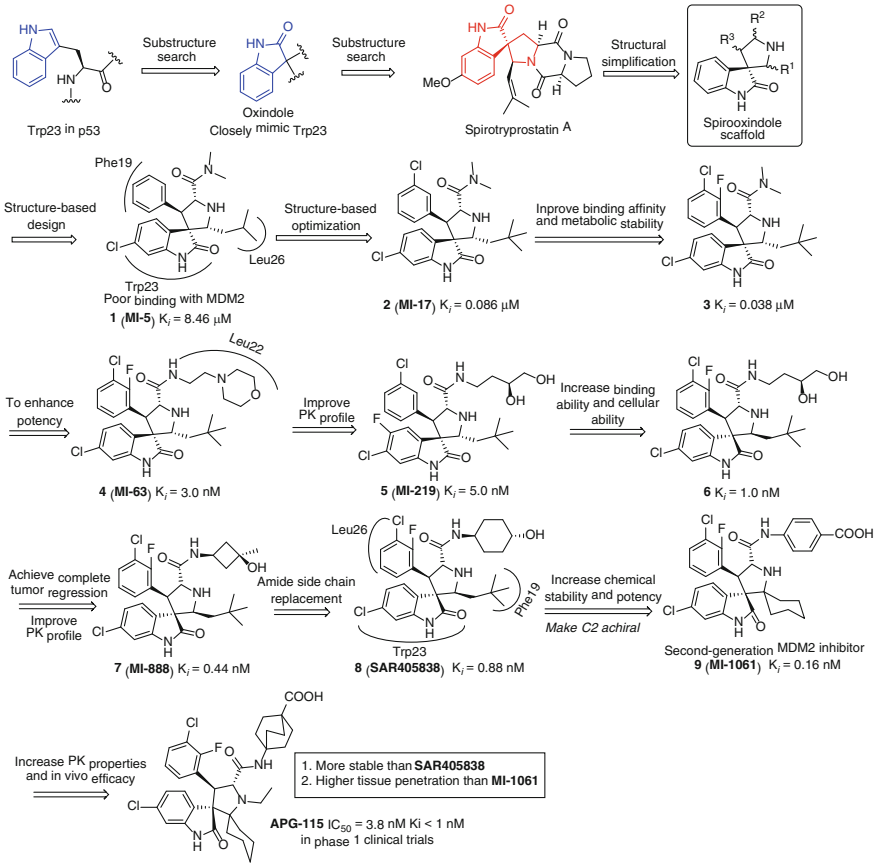

Fig. 8.4 Substructure-based discovery of spirooxindole-derived MDM2 inhibitors **SAR405838** and **APG-115** in clinical trials

core was inserted into the Trp23 cavity. Variations of substituents on the phenyl ring coupled with replacement of isopropyl with larger neopentyl group generated compound **2** (MI-17), which showed significantly increased binding affinity (K_i = 0.086 μM, about 100-fold more potent than MI-5) [59]. It is well believed that adding fluorine atom to the parent compounds can improve the physico-chemical properties (the acidity, lipophilicity, etc.), thus affecting the ADME properties [60]. Therefore, the fluorine atom was introduced into the phenyl ring of compound **2**, yielding compound **3**, which displayed improved binding affinity to MDM2 (K_i = 0.038 μM) [61]. Although compounds **1–3** displayed high binding affinities to MDM2, they were still less potent than the most potent p53-based peptide inhibitor (K_i = 1 nM) [59]. This suggests compound **3** may fail to occupy additional cavities that are crucial for the MDM2–p53 interactions. The X-ray analysis of MDM2–p53 complex together with mutant analysis [62] and alanine

scanning of p53 peptide [63] proved that aside from Trp23, Phe19, and Leu26, Leu22 was another important residue that was involved in the overall MDM2–p53 interactions. To mimic this additional Leu22 residue, the dimethylamine group in compound **3** was replaced with more hydrophilic morpholin-4-yl-ethylamine group to form MI-63 (compound **4**, K_i = 3.0 nM), where the carbon atoms in morphine ring and carbon linker closely mimicked Leu22 in p53 and the oxygen atom in morphine ring provided an additional hydrogen bond with positively charged Lys90 in MDM2. However, MI-63 had a poor PK profile, which hampered further in vivo evaluation [64]. Further modifications of the amide side chain and substituents on the phenyl ring and oxindole core of MI-63 yielded compound **5** (MI-219), which was endowed with increased oral bioavailability. Interestingly, although MI-219 potently inhibited MDM2 and reactivated p53 in cells expressing p53, there was no remarkable toxicity against normal cells with minimal p53 accumulation [64].

Compared to MI-219, compound **6** showed better binding affinity to MDM2 (K_i = 1 nM, comparable binding affinity with the most potent p53-based peptide inhibitor) and improved cellular ability, highlighting the importance of substituents on the phenyl rings and the stereochemistry [65]. Both MI-219 and compound **6**, however, failed to achieve complete tumor regression. In order to improve its PK profiles and in vivo antitumor potency, the diol side chain was replaced with the conformationally constrained *tert*-alcohol, yielding orally active compound **7** (MI-888, K_i = 0.44 nM), which achieved complete and durable tumor regression in two types of xenograft models [66]. Besides, the *tert*-alcohol group in MI-888 was proven to be able to block the CYP450 oxidation.

The stereochemistry, in some cases, plays an important role in the activity. Different enantiomer may have remarkably different binding affinity to their targets as observed in many drug molecules [45]. It is evident that spirooxindoles have multiple adjacent stereocenters, and different diastereoisomers may exist in the buffer solution of the biological testing. From the structural point of view, the diastereoisomer with all *trans*-configuration should be the most stable one because of the spatial repulsion of adjacent large groups. Indeed, isomerizations through the reversible ring-opening cyclization reaction of spirooxindoles in protic solvents such as MeOH, MeCN, H_2O were observed by some research groups [65–67], resulting in an equilibrium mixture of four diastereoisomers, as shown in MI-888 (Fig. 8.5). Compared to compound **10** (K_i = 4.5 nM), MI-888 had about tenfold binding affinity toward MDM2 (K_i = 0.44 nM), which suggests that three *trans*-configured hydrophobic substituents attached to the pyrrolidine ring in MI-888 may better mimic three key amino acid residues in p53 to occupy three hydrophobic cavities in MDM2. The structural requirement of all *trans*-configuration for optimal binding ability is probably due to the *a*-helical structure of *N*-domain of p53, in which Phe19, Trp23, and Leu26 residues may have similar *trans*-like spatial projection.

Replacement of the *tert*-alcohol group with a *trans*-4-hydroxycyclohexylamino group yielded SAR405838 (compound **8**, K_i = 0.88 nM), which is currently undergoing phase 1 clinical assessment for the treatment of human tumors retaining p53 (ClinicalTrials.gov Identifier for SAR405838: NCT01636479 and

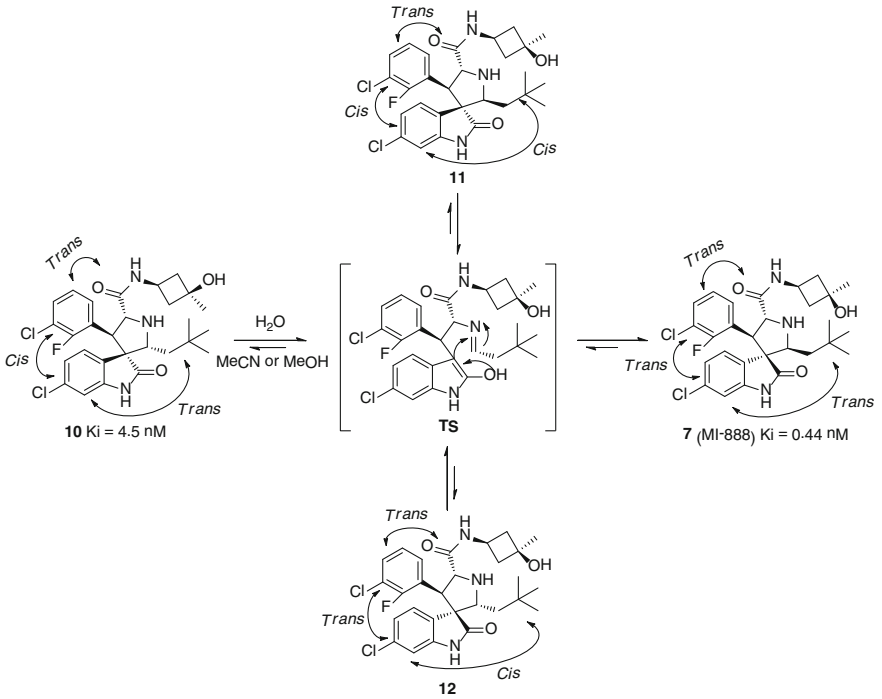

Fig. 8.5 Isomerization of spirooxindole **10** in protic solvents

NCT01985191) [33]. SAR405838 achieved complete and durable tumor regression in four types of xenograft models and induced strong apoptosis by up-regulating PUMA transcription. Very recently, Wang's group found that prolonged treatment of SJSA-1 tumor cells with SAR405838 induced different degrees of acquired resistance in vitro and in vivo, and the in vitro resistance was due to the mutation of DNA-binding domain of p53 and cannot be further activated by SAR405838 [68]. This type of acquired resistance in vitro and in vivo in acute leukemia RS4;11 and MV4;11 cell lines through mutation of the TP53 gene was also observed [69].

In terms of the binding model, the co-crystal structure of SAR405838-MDM2 complex showed that SAR405838 not only mimicked the three key residues (Phe19, Trp23, and Leu26) in p53, but also captured additional interactions that were not observed in MDM2–p53 interactions. The Cl atom in the oxindole ring was beneficial for its hydrophobic interaction with MDM2. The π–π interaction between His96 and the 2-fluoro-3-chlorophenyl group was observed, along with a hydrogen bond between the imidazole side chain of His96 and the amide carbonyl group of the hydrophilic chain (Fig. 8.6a). Besides, SAR405838 can also induce refolding of the *N*-terminal domain of MDM2 (residues 10–18) to achieve high binding through Val14 and Thr16 [33]. By contrast, structurally different MI-219 had different binding model with MDM2. The neopentyl and 3-Cl phenyl groups in

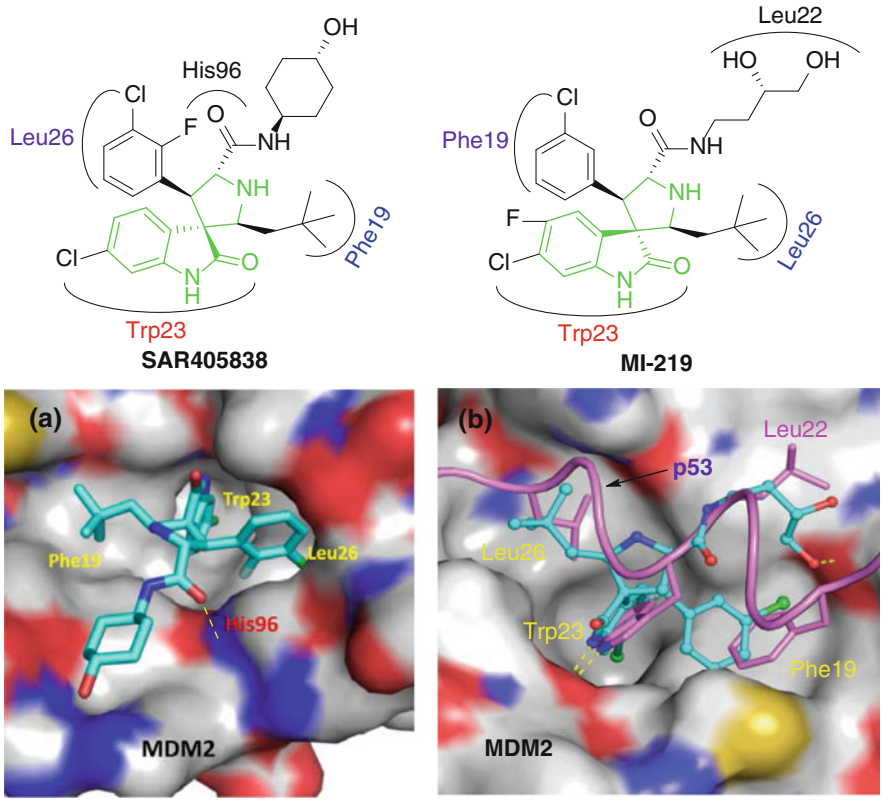

Fig. 8.6 Binding models of MI-219 and SAR405838 with MDM2 (PDB code: 1YCR). Reprinted with permission from Ref. [13]. Copyright © 2014, American Chemical Society

MI-219 mimicked Leu26 and Phe19 residues, respectively, to occupy corresponding cavities in MDM2 (Fig. 8.6b) [64]. Clearly, SAR405838 and MI-219 possessed the same structural scaffold (highlighted in green in Fig. 8.6). Carlos Garcia-Echeverria et al. also observed this kind of difference in binding models of spirooxindoles to MDM2 [70]. This different binding model of MI-219 may explain the suboptimal binding affinity to MDM2 compared to SAR405838 (5.0 nM for MI-219 vs. 0.88 nM for SAR405838).

As shown in Fig. 8.5, spirooxindoles can isomerize through the ring-opening retro-Mannich reaction in protic solvents to give a mixture of four diastereoisomers. Among them, the most potent MDM2 inhibitor is the one with all *trans*-configuration as shown in SAR405838. Based on this, Wang et al. designed a series of second-generation spirooxindoles as MDM2 inhibitors by introducing symmetric C2 substitution on the pyrrolidine ring [58]. Further modifications focusing on variations of C2 substituents and hydrophilic amide chains led to the discovery of MI-1061 (compound **9**, Fig. 8.4), which exhibited excellent chemical stability in

solutions and improved binding affinity to MDM2 (K_i = 0.16 nM), and induced apoptosis in the SJSA-1 xenograft model. Compared to the first-generation inhibitors, the second-generation possessed better binding affinity to MDM2. PK studies showed that MI-1061 had considerably lower C_{max} and AUC values than compound SAR405838 upon oral administration, indicating that further improvement of oral PK is needed for stronger in vivo antitumor activity [43]. Further structural modifications for improving tissue penetration were then carried out through decreasing the lipophilicity, reducing the acidity of carboxylic acids, increasing the basicity of the nitrogen atom in the pyrrolidine core, and finally leading to the discovery of APG-115, which is currently undergoing clinical assessment in patients with advanced solid tumor or lymphoma (ClinicalTrials.gov identifier for APG-115: NCT02935907). APG-115 showed extremely high binding affinity to MDM2 with the IC_{50} and K_i of 3.8 nM and <1 nM, respectively, and activated p53 in the SJSA-1 xenograft mice models following a single oral administration. Significantly, APG-115 achieved complete and long-lasting growth inhibition of the SJSA-1 xenograft tumors in mice and demonstrated strong antitumor efficacy in the RS4;11 acute leukemia model.

In addition to Wang's work, Yuuichi et al. also designed a series of spiropyrrolidinyl oxindole-based MDM2 inhibitors [71]. Their modifications focused on the variations of amide side chains and C2 substituents, as well as the bioisosteric replacement of phenyl ring with the pyridine ring, generating a library of structurally interesting and biologically important molecules as shown in Fig. 8.7. Apparently, these structures are highly similar to the drug candidates SAR405838, RO8994 (as shown in Fig. 8.4 and Fig. 8.8, respectively), and their second-generation inhibitors (MI-1061, RO2468, and RO5353), reported by Wang and Graves's group in 2013–2014. Intriguingly, all these structures had symmetric C2 substituents (highlighted in bold in scaffold **13** in Fig. 8.7), which were subsequently proved to be crucial for improving chemical stability of such scaffolds and binding affinities to MDM2, leading to the identification of second-generation MDM2 inhibitors such as MI-1061 [58, 72]. However, the inventors of this patent just claimed these compounds can be used as antitumor agents through disrupting MDM2–p53 interactions without detailed biological data reported.

Apart from the spirooxindole-based MDM2 inhibitors (known as MI series), the Graves group identified another series of MDM2 inhibitors, such as RG7388, RO8994, RO2468, and RO5353 (Fig. 8.8). Among them, RG7388 is currently undergoing phase 1 clinical evaluation for the treatment of solid and hematological tumors (ClinicalTrials.gov Identifier for RG7388: NCT02407080).

This program was initiated to identify new MDM2 inhibitors with novel scaffolds, in which two aryl groups (A and B in compound **21**) are '*trans*' to each other, different from that in RG7112 (a drug candidate in phase 1 clinical trials belonging to Nutlin family as shown in Fig. 8.2) and MI-219. Much less is known regarding the effect of this *trans*-configuration of pyrrolidine core toward the binding affinity to MDM2. Based on the structures of RG7112 and MI-219 (A and B rings in both compounds are '*cis'* to each other), they designed and synthesized the MDM2 inhibitor compound **21** (IC_{50} = 196 nM), which was less potent than RG7112 (IC_{50} = 18 nM) but

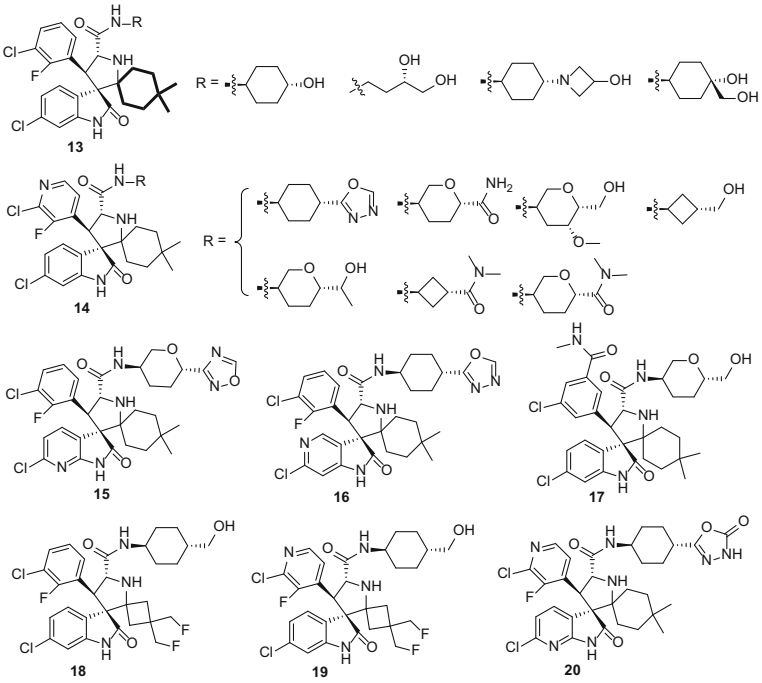

Fig. 8.7 Spirooxindoles and their bioisosteres as MDM2 inhibitors

significantly more potent than its enantiomer (IC_{50} > 10,000 nM) [42]. The introduction of fluorine atom to both phenyl rings yielded compound **22** with improved binding affinity to MDM2 (IC_{50} = 74 nM). Unfortunately, compounds **21** and **22** were found to have poor oral bioavailability and high clearance rates in mouse PK studies. The diol side chain could be oxidized in the metabolic process, so further modifications focusing on the diol side chain were performed, generating a new series of analogs with diverse amide side chains. Of these compounds, compound **23** with the *p*-benzoic acid group showed markedly increased PK profiles and cellular potency/selectivity (IC_{50} = 22 nM), showing promise for further optimizations. Subsequent modifications by introducing electron-donating or withdrawing groups to the phenyl ring eventually led to the discovery of RG7388 (compound **24**, IC_{50} = 6 nM).

Very recently, RG7388 was reported to be able to enhance the activity of ionizing radiation (XRT) in xenograft models of childhood sarcoma without inducing extra local XRT skin toxicity [73]. Combination of the key structural units of RG7388 with the oxindole scaffold gave compound **25**, which shared the same structural architecture with SAR405838 with a slight difference in the amide side chain [74]. However, compound **25** was also found to have a high clearance rate (34.6 mL/min/kg) and suboptimal oral bioavailability (F = 21), albeit with impressive cellular potency (IC_{50} = 5 nM). In order to improve the PK properties,

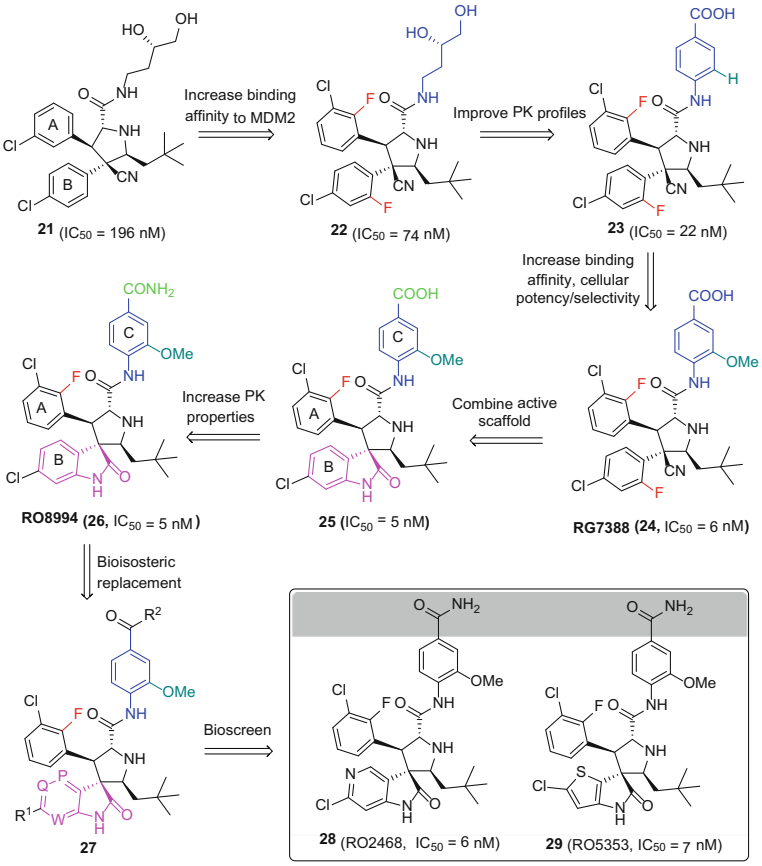

Fig. 8.8 Identification of drug candidate RG7388 and further optimizations

further optimization of compound **25** by converting the terminal carboxylic acid group to carboxamide group yielded RO8994 (compound **26**), which exhibited significantly decreased clearance rate (5.8 mL/min/kg) and improved oral bioavailability (F = 92). Besides, the aromatic group C in both RG7388 and RG8994 can markedly improve the metabolic stability, PK properties, cellular potency/selectivity, and in vivo efficacy, compared to MI-888 with an aliphatic amide side chain [62, 63]. RG7388 and RO8994 dose-dependently and non-genotoxically induced p53 stabilization, cell cycle arrest, and apoptosis in tumor cells retaining wt p53. An impressive in vivo efficacy for RG7388 and RO8994 against human SJSA1 tumor xenografts was observed at significantly lower doses and exposures, more efficacy than RG7112 and MI-888. The interaction between 6-chlorooxindole group and the Trp23 subpocket is believed to be the most crucial. Further derivatizations of RO8994 on the 6-chlorooxindole motif using bioisosteric replacement strategies were carried out in the Graves group,

generating a new series of RO8994 analogs as shown in **27** (Fig. 8.8) [75]. Among this series, RO2468 (compound **28**) and RO5353 (compound **29**) showed promise for clinical development with excellent PK profiles, impressive in vivo efficacy in SJSA1 xenograft models, and excellent cellular potency/selectivity. Additionally, computational docking studies showed that this series of compounds had similar binding models with SAR405838. The 6-chlorooxindole motif occupied the Trp23 pocket with the NH forming a hydrogen bond with the backbone carbonyl of MDM2, while the 2-fluoro-3-chloro phenyl group and the neopentyl group were filled into Leu26 and Phe19 hydrophobic pockets, respectively. In order to exhibit their anticancer potential for clinical development, the preclinical data of RG7388, RO8994, RO2468, and RO5353 are summarized in Table 8.1.

Apart from those discussed above, the Graves group also designed other series of spirooxindoles as MDM2 inhibitors (Fig. 8.9). Initially, they found that only the (*S*)-**30** was active with an IC_{50} of 3.9 μM in a biochemical binding assay [76]. This moderate binding affinity may be attributed to the suboptimal binding of acylated piperidine group to the Phe19 pocket, although the 6-chlorooxindole motif can occupy the deep and narrow Trp23 pocket in MDM2. Further structural rigidization through cyclization strategies gave a library of small molecules with different scaffolds [77–82]. Of these scaffolds, scaffolds 2 and 4 (highlighted in blue in Fig. 8.9) failed to progress because of unfavorable physicochemical or pharmaceutical properties, albeit with enhanced binding affinities. For the remaining scaffolds, they just claimed that these compounds can serve as antitumor agents by targeting MDM2, but no further information has been reported since then. Compared to those with pyrrolidine core such as SAR405838 and RG7388, the suboptimal binding affinities of these scaffolds to MDM2 in Fig. 8.9 are probably attributed to their structural features. In contrast to 6- or 7-membered ring systems, 5-membered pyrrolidine ring systems are generally more flexible because of their

Table 8.1 Preclinical data of RG7388, RO8994, RO2468, and RO5353

Compound	RG7388	RO8994	RO2468	RO5353
MTT IC_{50} (μM)[a]	0.03	0.02	0.015	0.007
HTRF IC_{50} (nM)[b]	6	5	6	7
HLM_CL (mL/min/kg)	4.3	7.5	10.2	2.0
PO dose (mg/kg)	50	25	5	10
PO AUC/dose (μg h/mL/mg/kg)	1.3	3.7	4.2	1.5
PO C_{max} (μg/mL)	9.9	5.8	2.1	1.3
IV dose (mg/kg)	5	0.64	2	2.5
CL (mL/min/kg)	10.3	5.8	1.8	9.9
$t_{1/2}$ (h)	1.6	7.1	3.0	3.0
F (%)	80	92	46	92

[a]Mean IC_{50} of three wt p53 cancer cell lines (SJSA, RKO, and HCT116)
[b]The binding affinity was determined by the homogeneous time-resolved fluorescence (HTRF) binding assay
[c]F represents oral bioavailability

pseudorotational mobility [83–87] and have two predominant puckering modes, namely the '*Cis–Cis*' and '*trans–trans*' models [88]. The '*trans–trans*' model has been proved to be crucial for optimal binding to MDM2 as shown in SAR405838 and RG7388, where the two aromatic rings (A and B rings in Fig. 8.8) adopt a *trans*-configuration. Evidently, scaffolds in Fig. 8.9 are rigid and cannot maintain a '*trans–trans*' configuration.

Aside from those discussed above that can inhibit MDM2–p53 interactions at nanomolar levels, other MDM2 inhibitors with different core structures (highlighted in red in Fig. 8.10) were also reported before. These MDM2 inhibitors may help us gain deeper insights into the structure–activity relationships (SARs) and design novel small-molecule inhibitors with excellent potency, selectivity, and low toxicity although these inhibitors showed moderate MDM2 inhibition (K_i > 1 μM). Isabel Gomez-Monterrey et al. designed a new series of indoline-3, 2'-thiazolidines as possible MDM2 inhibitors from the imidazo-[1, 5-*c*] thiazole scaffold (Fig. 8.10), similar to scaffold 7 in Fig. 8.9 [89]. Initially, they proposed that the imidazo-[1, 5-*c*] thiazole scaffolds such as compound **32** could define the orientation of oxindole, aryl, and alkyl groups to mimic the three key residues (Trp23, Phe19, and Leu26) in p53. Compound **32** showed good cytotoxicity against HEK, M14, and U937 cancer cell lines (IC_{50} < 1 μM) and increased p53 expression. NMR studies showed compound **32** can block MDM2–p53 interactions, but was less potent than Nutlin-3. Subsequent modifications with the aim of reducing conformational constraints by the ring-opening of imidazolone gave compound **33**, which exhibited excellent cytotoxicity against a panel of human cancer cell lines, especially for

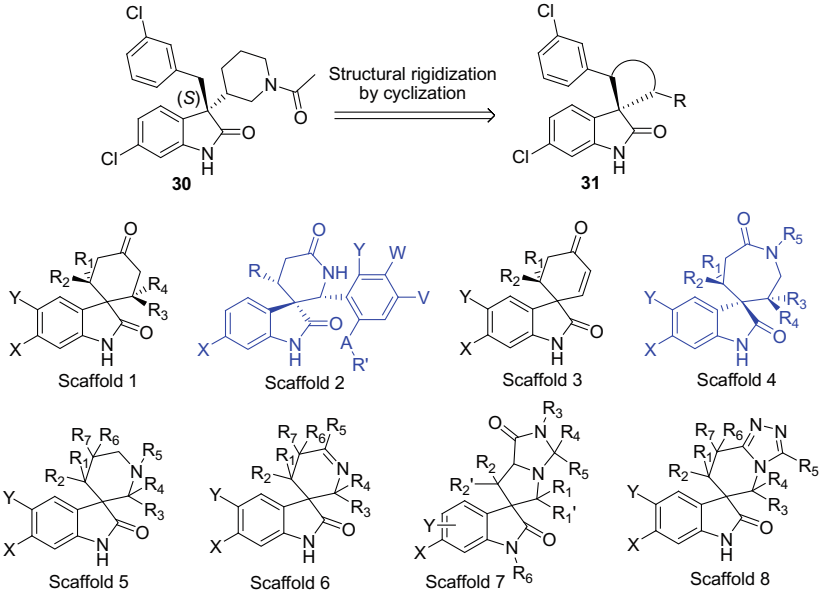

Fig. 8.9 Structurally rigid spirooxindoles as possible MDM2 inhibitors

MCF-7, U937, and HT29 cell lines with the IC_{50} values of 0.04, 0.07, and 0.07 μM, respectively. However, certain cytotoxicity against human normal cell line HGF was also observed (IC_{50} = 1.60 μM). The immunoprecipitation assay indicated that compound **33** inhibited 30% of MDM2–p53 interactions. Docking studies showed that the cyclohexyl carbonyl and ethyl ester groups occupied the Trp23 and Phe19 pockets, respectively, while the oxindole core was inserted into the Leu54 pocket, not the Leu26. The hydrolysis of ester group resulted in a loss of activity as the hydrophilic acid group cannot be filled into the hydrophobic Phe19 cavity.

Very recently, Ivanenkov and co-workers designed dispiro-indolinones by combining the spirooxindole and 2-thiohydantoin moiety [90]. The most potent compound **34** (diastereomeric mixture) among this series showed good inhibitory activity against several cancer cell lines of different origins with the IC_{50} values

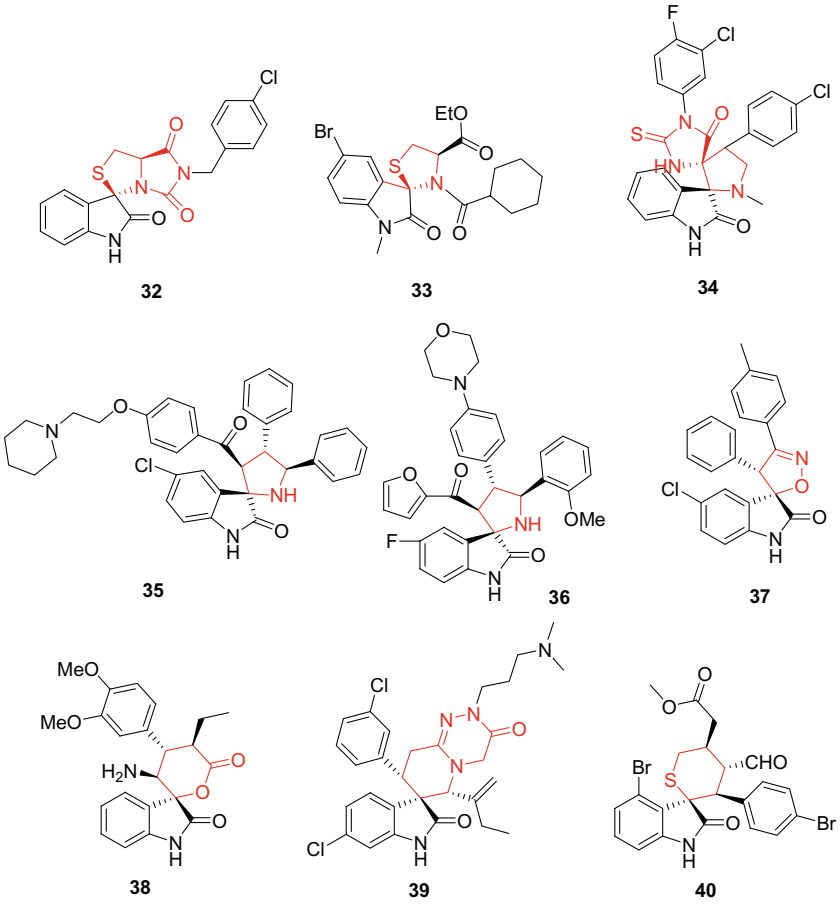

Fig. 8.10 Other reported spirooxindole-based MDM2 inhibitors

ranging from 4.88 to 9.08 μM (IC_{50} = 4.88 μM against MCF-7 cells). No selectivity, however, toward HCT116 ($p53^{+/+}$) and HCT116 ($p53^{-/-}$) was observed. Compound **34** was less potent and selective than Nutlin-3a. Based on the 2D structural similarity analysis of reported MDM2 inhibitors and docking results, the authors proposed that MDM2 could be the main target of their compounds.

Previously reported potent MDM2 inhibitors such as Nutlins, AM8553, MI family, and RG7388 possess diaryl substituents around the pyrrolidine ring. Based on the structural features, Kumar et al. designed a series of diaryl-spirooxindoles having the spiro [indoline-3, 2′-pyrrolidin]-2-one scaffold, which were bioisosteres of MI-63 (as shown in Fig. 8.4) [91]. Of this series, compound **35** (Fig. 8.10) exhibited the best inhibition against breast cancer cell lines MCF-7 and MDA-MB 231 with the IC_{50} values of 3.7 and 6.5 μM, respectively, more potent than Nutlin-3 and OH-Tamoxifen. Also, good selectivity was observed (IC_{50} > 50 μM against HEK-293 and VERO cells). Further mechanism studies showed that compound **35** displayed excellent in vivo antitumor activity in wt p53 containing MCF-7 xenograft model in nude mice by restoring p53 function (66% lower in tumor volume and size than that of vehicle group at 20 mg/kg after 14-day treatment) and modulated downstream proteins p21, pRb, and CCND1. Structurally similar compound **36** designed by He and co-workers inhibited growth of MDM2 overexpressed LNCaP cells with an IC_{50} value of 0.35 μg/mL [92].

Santos's group synthesized spiroisoxazoline oxindoles, where three hydrophobic groups (two phenyl rings and the oxindole core) were designed to mimic three key residues Phe19, Leu26, and Trp23 in p53 [93]. Compound **37** was found to be the most potent one against HepG2 expressing wt p53 with an GI_{50} value of 29.11 μM, about twice potent than Nutlin-3 (GI_{50} = 51.31 μM). The BiFC (venus-based bimolecular fluorescence complementation) assay indicated compound **37** inhibited MDM2–p53 interactions and dose-dependently induced expression of cleaved PARP and active caspase-3.

Compound **38** designed by Peng et al. bonded to MDM2 moderately (K_i = 0.21 μM) and selectively inhibited growth of HCT116 ($p53^{+/+}$) and PC-3 ($p53^{-/-}$) cells with the IC_{50} values of 2.26 and 25.16 μM, respectively, while compound **39** was found to be able to dock into MDM2 pockets [94]. Very recently, Han et al. reported that chroman-fused spirooxindoles with spirohexyl oxindole scaffold can potently inhibit growth of an array of cancer cells (IC_{50} = 1.7 μM against MCF-7) by blocking the MDM2–p53 interactions and downstream pathways [95]. Sheng et al. identified a series of structurally novel tetrahydrothiopyran fused spirooxindoles using the organocatalysis strategy, which showed good cytotoxicity through interrupting the p53–MDM2 interactions [96]. Among these compounds, compound **40** potently inhibited growth of A549, HCT116, and MDA-MB-231 cells with the IC_{50} values ranging from 1.57 to 3.55 μM. The MDM2 inhibition of compound **40** was further confirmed by the fluorescence polarization and Western blotting assays, showing that compound **40** inhibited MDM2 with a K_D value of 2.2 μM and up-regulated expression of p53 and MDM2 in A549 cells concentration-dependently. Docking simulations showed that the oxindole, methyl ester, and bromophenyl groups occupied the Leu26,

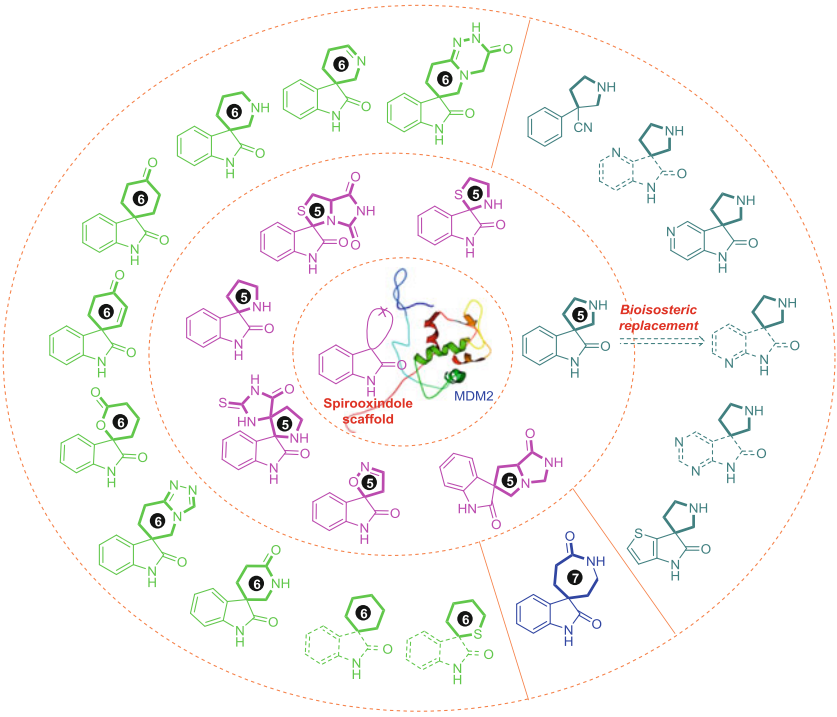

Fig. 8.11 An overview of spirooxindole-based scaffolds as MDM2 inhibitors

Phe19, and Trp23 cavity of MDM2, respectively. It is worth noting that this series of compounds also possessed modifiable synthetic handles (e.g., the ester and aldehyde moiety), which could be utilized for late-stage structural modifications to search more potent MDM2 inhibitors for anticancer treatment.

Based on previously reported small-molecule inhibitors of MDM2–p53 interactions discussed above, the structural scaffolds of spirooxindole-based MDM2 inhibitors are summarized in Fig. 8.11 (substituents attached to the scaffolds are omitted).

8.2.2 Summary on SARs

On the basis of above analysis, it is evident that potent spirooxindole-based MDM2 inhibitors such as SAR405838, APG-115, RO8994, and RG7388 possess scaffolds **41** and **42**. Scaffold **42** can be regarded as the ring-opening bioisostere of scaffold **41** (Fig. 8.12). The general trend of SARs related to scaffold **41** was consistent with that of scaffold **42**, and the cyano group of scaffold **42** was found to be critical for maintaining the *trans*-configuration of A and B rings [42].

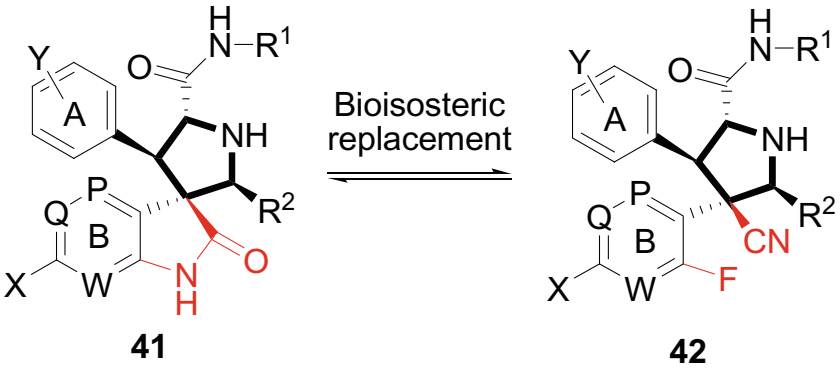

Fig. 8.12 General scaffolds of spirooxindoles and their bioisosteres as MDM2 inhibitors

For spirooxindole-based MDM2 inhibitors and their bioisosteres, the SARs are summarized below, although this summary may be not comprehensive.

(a) **The structure scaffold** (highlighted in bold in scaffolds **41** and **42**). The saturated 5-membered rings, the pyrrolidine ring in particular, are more preferred than structurally rigid 6-/7-membered rings (as shown in Fig. 8.9) and unsaturated 5-membered rings (as shown in compound **37** in Fig. 8.10) as saturated 5-membered rings are more flexible to maintain the '*trans–trans*' configuration (as shown in SAR405838, RG7388, etc.), which has been proved to be crucial for optimal binding to MDM2. The pyrrolidine ring seems to be the optimal structural unit for designing spirooxindole-based MDM2 inhibitors to date. However, much less is known about the function of NH unit in pyrrolidine in binding affinity to MDM2. Recent work by Wang et al. showed the addition of ethyl group to the nitrogen atom improved the chemical stability [43]. Other 5-membered rings such as tetrahydrofuran, tetrahydrothiophene, cyclopentane have not yet been investigated.

(b) **The stereochemistry**. Substituents around the pyrrolidine core should be '*trans*' to each other for optimal binding. Variations of configurations may result in suboptimal binding affinities to MDM2 (K_i = 4.5 and 0.44 nM for compound **10** and MI-888, respectively, as shown in Fig. 8.5) and different binding models with MDM2 (as shown in Fig. 8.6). The *trans*-substituents can better mimic three key residues (Phe19, Trp23, and Leu26) in p53 to occupy hydrophobic subpockets on the surface of MDM2. This preferred *trans*-configuration could be explained by the *a*-helical structure of *N*-terminal domain of p53, where three key residues are '*trans*' to each other. Besides, compounds with all *trans*-configurations are more chemically stable in protic solvents.

(c) **The R^2 group**. Larger aliphatic groups may be preferred over smaller ones. The binding affinities of inhibitors to MDM2 increase following the order: cyclohexyl (in MI-1061) > neopentyl (in SAR405838) > 2-isobutyl (in MI-5). Large groups may fit well into the Phe19 hydrophobic pocket with improved binding

affinities. Little known is about the effect of aromatic rings on the binding affinities, although the aromatic ring can better mimic the Phe19 residue (as depicted in Fig. 8.3c). Also, the introduction of symmetric substituents (e.g., the cyclohexyl group in MI-1061) can increase the chemical stability by irreversible isomerization in protic solvents.

(d) **The oxindole core**. The oxindole core in scaffold **41** or the phenyl ring (B) in scaffold **42** occupies the deep and narrow Trp23 pocket, which is the most crucial for blocking MDM2–p53 interactions. The NH in the oxindole core forms a hydrogen bond with the backbone carbonyl in MDM2. Modifications on the NH position may result in decreased binding affinity. The chlorine atom at the 6-position of the oxindole core is beneficial for enhancing binding affinity because of the additional interaction of 6-Cl with the Trp23 cavity. Bioisosteric replacement of the phenyl ring with pyridine or thiophene gives comparable binding affinity but with improved cytotoxicity as shown in Table 8.1 (RO8994 *vs* RO2468 and RO5353) [75]. Replacement of phenyl ring with pyridinyl ring leads to significantly decreased oral bioavailability (RO8994 vs. RO2468). The position of nitrogen atom in the pyridine ring in scaffold **41** is important for the binding affinity and cytotoxicity. When P or W in scaffold **41** is the nitrogen atom, the binding ability and cytotoxicity decrease accordingly. The fluorine atom in scaffold **42** can improve binding ability to MDM2.

(e) **The A ring in Scaffolds 41 and 42**. The phenyl ring (A) in these two types of scaffolds has been proved to be inserted into the Leu26 pocket in MDM2. Also, the π–π interaction between His96 and the phenyl ring has been observed and is crucial for enhancing binding affinity to MDM2. Therefore, the substituent without the π-system would be less favored. The introduction of fluorine and chlorine atoms into the 2- and 3-position, respectively, can improve binding affinity and metabolic stability.

(f) **The amide side chain**. In contrast to the aliphatic amide side chains (as shown in MI series), the introduction of the aromatic side chain (as shown in RO8994 in Fig. 8.8) can markedly improve the metabolic stability, PK properties, cellular potency/selectivity, and in vivo efficacy. Among the aromatic groups, the introduction of the terminal benzamide group can reduce the clearance rates and improve oral bioavailability compared to the benzoic acid group (RO8994 *vs.* compound **25** in Fig. 8.8). Besides, the amide carbonyl group forms a hydrogen bond with His96. The ester group may be less preferred than the amide group as the ester group is not stable enough and may undergo the enzymatic hydrolysis under the physiological conditions. More importantly, a hydrophilic amide side chain (solvent-exposed polar group) is necessary to protect the hydrophobic interface between MDM2 and inhibitors from surrounding solvent [97]. Lack of this hydrophilic moiety may cause suboptimal binding affinity. Most of the potent small molecules that disrupt MDM2–p53 interactions possess a hydrophilic amide side chain as shown in drug candidates in Fig. 8.2. It is believed that the solvent-exposed polar group can provide additional interactions that are outside the MDM2–p53 interactions. For example, the diol group in MI-219 can contact with Leu22 as shown in Fig. 8.6.

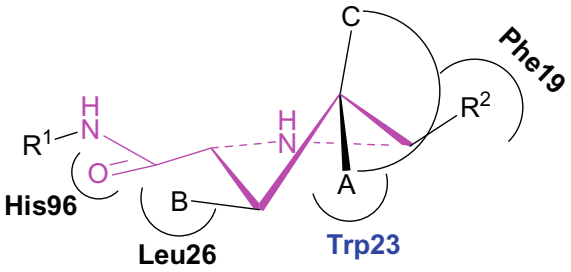

Fig. 8.13 Prolinamide-based '3+1' model for designing potent MDM2 inhibitors

On the basis of above SARs analysis, we tentatively propose the prolinamide (highlighted in purple in Fig. 8.13)-based '3+1' model for designing potent MDM2 inhibitors based on the following considerations: (1) the amide carbonyl group in prolinamide has an additional interaction with His96 through a hydrogen bond, which is beneficial for improving binding affinity; (2) the pyrrolidine ring of prolinamide can maintain the required '*trans–trans*' configuration for optimal binding to MDM2 due to its pseudorotational mobility. The '3' refers to the three hydrophobic moieties (R^2, A, and B) that are designed to occupy the Phe19, Trp23, and Leu26 subpockets, respectively, in MDM2. The 'B' group with a π-system can interact with His96 near the Leu26 pocket through the π–π stacking. It should be noted that a cyclic unit (e.g., the oxindole core in SAR405838) formed by A and C can also fit well into the Trp23 cavity. The '1' refers to the hydrophilic amide side chain (R^1), which may capture additional interactions.

8.3 Conclusions and Outlooks

Spiro compounds have drawn unprecedented attention in drug discovery because of its prevalence in natural products and the 3D structural features. It is well believed that non-flat spiro compounds can specifically bind to biological targets with reduced conformational entropy. All these features make spiro scaffolds attractive starting points in drug discovery programs.

Historically, disruption of PPIs is always challenging as PPIs generally involve a large and flat interface. Differently, the MDM2–p53 interactions are primarily mediated by three key residues (Trp23, Phe19, and Leu26), and this well-defined fashion has provided a rationale for designing non-peptide small-molecule inhibitors. Particularly, spirooxindole scaffolds have shown diverse bioactivities and have been observed in drug leads such as SAR405838 (MDM2 inhibitor), CFI-400945 (the first PLK4 inhibitor), and KAE609 (antimalarial agent) as well as natural products. Interestingly, spirooxindoles are privileged scaffolds in identifying potent MDM2 inhibitors, and several potent MDM2 inhibitors (SAR405838, RO8994, etc.) derived from spirooxindoles are currently in preclinical or clinical trials. After scaffold analysis, we found that 5-membered rings fused at C-3 position,

the pyrrolidine ring in particular, are more preferred than structurally rigid 6/7-membered rings for optimal binding affinity to MDM2 because of the pseudorotational mobility of pyrrolidine ring. Based on the SARs analysis and binding models of MDM2 inhibitors to MDM2 protein, we tentatively proposed the prolinamide-based '3+1' model, which may be regarded as the general template for designing small molecules interrupting the MDM2–p53 interactions.

In general, potent MDM2 inhibitors should possess three hydrophobic groups and one hydrophilic group. The hydrophobic groups mimic three key residues Phe19, Trp23, and Leu26 in p53 to occupy cavities in MDM2, while the hydrophilic group exposed to the solvent region can protect the hydrophobic interaction surface between MDM2 and potent inhibitors from surrounding solvent and provide extra interactions that are out of MDM2–p53 interaction for optimal binding ability. Although several MDM2 inhibitors have entered phase 1 clinical trials for anticancer treatment, challenges still exist and should be addressed further. Acquired resistance to these MDM2 inhibitors has been observed after prolonged treatment. Therefore, the development of new MDM2 antagonists for the newly occurred mutations and combinations of MDM2 inhibitors with other agents that are effective against p53-mutated cancer cells are promising strategies against the acquired resistance. Another challenge is the toxicity of these MDM2 inhibitors to normal tissues as p53 is expressed in all proliferative cells and plays pivotal roles in regulating normal cellular processes. The activation of p53 in normal cells may result in unwanted side effects or even toxicity. Appropriate dose regimes that maintain strong inhibitory activity but with less toxicity to normal tissues would alleviate the toxicity.

Acknowledgements This work was supported by the National Natural Science Foundation of China (No. 81430085, 21372206, and 81703326, National Key Research Program of Proteins (No. 2016YFA0501800), Key Research Program of Henan Province (No. 1611003110100), Scientific Program of Henan Province (No. 182102310123), China Postdoctoral Science Foundation (No. 2018M630840), Key Research Program of Higher Education of Henan Province (No.18B350009), and the Starting Grant of Zhengzhou University (No. 32210533).

References

1. Bieging KT, Mello SS, Attardi LD (2014) Unravelling mechanisms of p53-mediated tumour suppression. Nat Rev Cancer 14:359–370
2. Wu X, Bayle JH, Olson D et al (1993) The p53-mdm-2 autoregulatory feedback loop. Genes Dev 7:1126–1132
3. Harris SL, Levine AJ (2005) The p53 pathway: positive and negative feedback loops. Oncogene 24:2899–2908
4. Chen F, Wang W, El-Deiry WS (2010) Current strategies to target p53 in cancer. Biochem Pharmacol 80:724–730
5. Moll UM, Petrenko O (2003) The MDM2-p53 Interaction. Mol Cancer Res 1:1001–1008
6. Feki A, Irminger-Finger I (2004) Mutational spectrum of p53 mutations in primary breast and ovarian tumors. Crit Rev Oncol Hematol 52:103–116

7. Momand J, Jung D, Wilczynski S et al (1998) The MDM2 gene amplification database. Nucleic Acids Res 26:3453–3459
8. Forslund A, Zeng Z, Qin L-X et al (2008) MDM2 gene amplification is correlated to tumor progression but not to the presence of SNP309 or TP53 mutational status in primary colorectal cancers. Mol Cancer Res 6:205–211
9. Dickens MP, Fitzgerald R, Fischer PM (2010) Small-molecule inhibitors of MDM2 as new anticancer therapeutics. Semin Cancer Biol 20:10–18
10. Barakat K, Mane J, Friesen D et al (2010) Ensemble-based virtual screening reveals dual-inhibitors for the p53–MDM2/MDMX interactions. J Mol Graph Model 28:555–568
11. Shangary S, Wang S (2009) Small-molecule inhibitors of the MDM2-p53 protein-protein interaction to reactivate p53 function: a novel approach for cancer therapy. Annu Rev Pharmacol Toxicol 49:223–241
12. Tanimura S, Ohtsuka S, Mitsui K et al (1999) MDM2 interacts with MDMX through their RING finger domains. FEBS Lett 447:5–9
13. Zhao Y, Aguilar A, Bernard D et al (2015) Small-molecule inhibitors of the MDM2–p53 protein-protein interaction (MDM2 inhibitors) in clinical trials for cancer treatment. J Med Chem 58:1038–1052
14. Brown CJ, Cheok CF, Verma CS et al (2011) Reactivation of p53: from peptides to small molecules. Trends Pharmacol Sci 32:53–62
15. Saha T, Kar RK, Sa G (2015) Structural and sequential context of p53: a review of experimental and theoretical evidence. Prog Biophys Mol Biol 117:250–263
16. Nero TL, Morton CJ, Holien JK et al (2014) Oncogenic protein interfaces: small molecules, big challenges. Nat Rev Cancer 14:248–262
17. Guo W, Wisniewski JA, Ji H (2014) Hot spot-based design of small-molecule inhibitors for protein–protein interactions. Bioorg Med Chem Lett 24:2546–2554
18. Kussie PH, Gorina S, Marechal V et al (1996) Structure of the MDM2 oncoprotein bound to the p53 tumor suppressor transactivation domain. Science 274:948–953
19. Vassilev LT, Vu BT, Graves B et al (2004) In vivo activation of the p53 pathway by small-molecule antagonists of MDM2. Science 303:844–848
20. Vassilev LT (2007) MDM2 inhibitors for cancer therapy. Trends Mol Med 13:23–31
21. Lv P-C, Sun J, Zhu H-L (2015) Recent advances of p53-MDM2 small molecule inhibitors (2011-Present). Curr Med Chem 22:618–626
22. Zak K, Pecak A, Rys B et al (2013) Mdm2 and MdmX inhibitors for the treatment of cancer: a patent review (2011–present). Expert Opin Ther Pat 23:425–448
23. Wang W, Hu Y (2012) Small molecule agents targeting the p53-MDM2 pathway for cancer therapy. Med Res Rev 32:1159–1196
24. Liu L, Bernard D, Wang S (2015) Case study: discovery of inhibitors of the MDM2–p53 protein-protein interaction. In: Meyerkord CL, Fu H (eds) Protein-protein interactions, vol 1278. Methods in molecular biology. Springer, New York, pp 567–585
25. Zhang B, Golding BT, Hardcastle IR (2015) Small-molecule MDM2-p53 inhibitors: recent advances. Future Med Chem 7:631–645
26. Hardcastle IR (2014) Targeting the MDM2–p53 protein-protein interaction: design, discovery, and development of novel anticancer agents. In: Neidle S (ed) Cancer drug design and discovery, 2nd edn. Academic Press, San Diego, pp 391–426
27. Popowicz GM, Dömling A, Holak TA (2011) The structure-based design of Mdm2/Mdmx–p53 inhibitors gets serious. Angew Chem Int Ed 50:2680–2688
28. Khoury K, Popowicz GM, Holak TA et al (2011) The p53-MDM2/MDMX axis—a chemotype perspective. MedChemComm 2:246–260
29. Lemos A, Leão M, Soares J et al (2016) Medicinal chemistry strategies to disrupt the p53–MDM2/MDMX interaction. Med Res Rev 36:789–844
30. Secchiero P, Bosco R, Celeghini C et al (2011) Recent advances in the therapeutic perspectives of Nutlin-3. Curr Pharm Design 17:569–577

31. Koblish HK, Zhao S, Franks CF et al (2006) Benzodiazepinedione inhibitors of the Hdm2: p53 complex suppress human tumor cell proliferation in vitro and sensitize tumors to doxorubicin in vivo. Mol Cancer Ther 5:160–169
32. Rew Y, Sun D, Yan X et al (2014) Discovery of AM-7209, a potent and selective 4-amidobenzoic acid inhibitor of the MDM2–p53 interaction. J Med Chem 57:10499–10511
33. Wang S, Sun W, Zhao Y et al (2014) SAR405838: an optimized inhibitor of MDM2–p53 interaction that induces complete and durable tumor regression. Cancer Res 74:5855–5865
34. Sun D, Li Z, Rew Y et al (2014) Discovery of AMG 232, a potent, selective, and orally bioavailable MDM2–p53 inhibitor in clinical development. J Med Chem 57:1454–1472
35. Canon J, Osgood T, Olson SH et al (2015) The MDM2 inhibitor AMG 232 demonstrates robust anti-tumor efficacy and potentiates the activity of p53-inducing cytotoxic agents. Mol Cancer Ther 14:649–658
36. Wang Y, Zhu J, Liu J et al (2014) Optimization beyond AMG 232: Discovery and SAR of sulfonamides on a piperidinone scaffold as potent inhibitors of the MDM2-p53 protein–protein interaction. Bioorg Med Chem Lett 24:3782–3785
37. Valat T, Masuya K, Baysang F et al (2014) Mechanistic study of NVP-CGM097: a potent, selective and species specific inhibitor of p53-Mdm2. Cancer Res 74:1798
38. Gessier F, Kallen J, Jacoby E et al (2015) Discovery of dihydroisoquinolinone derivatives as novel inhibitors of the p53–MDM2 interaction with a distinct binding mode. Bioorg Med Chem Lett 25:3621–3625
39. Holzer P, Masuya K, Furet P et al (2015) Discovery of a dihydroisoquinolinone derivative (NVP-CGM097): a highly potent and selective MDM2 inhibitor undergoing phase 1 clinical trials in p53wt tumors. J Med Chem 58:6348–6358
40. Tovar C, Graves B, Packman K et al (2013) MDM2 small-molecule antagonist RG7112 activates p53 signaling and regresses human tumors in preclinical cancer models. Cancer Res 73:2587–2597
41. Vu B, Wovkulich P, Pizzolato G et al (2013) Discovery of RG7112: a small-molecule MDM2 inhibitor in clinical development. ACS Med Chem Lett 4:466–469
42. Ding Q, Zhang Z, Liu J-J et al (2013) Discovery of RG7388, a potent and selective p53–MDM2 inhibitor in clinical development. J Med Chem 56:5979–5983
43. Aguilar A, Lu J, Liu L et al (2017) Discovery of 4-((3′R,4′S,5′R)-6″-Chloro-4′-(3-chloro-2-fluorophenyl)-1′-ethyl-2″-oxodispiro[cyclohexane-1,2′-pyrrolidine-3′,3″-indoline]-5′-carboxamido)bicyclo[2.2.2]octane-1-carboxylic Acid (AA-115/APG-115): a potent and orally active Murine Double Minute 2 (MDM2) inhibitor in clinical development. J Med Chem 60:2819–2839
44. Over B, Wetzel S, Grütter C et al (2013) Natural-product-derived fragments for fragment-based ligand discovery. Nat Chem 5:21–28
45. Galliford CV, Scheidt KA (2007) Pyrrolidinyl-spirooxindole natural products as inspirations for the development of potential therapeutic agents. Angew Chem Int Ed 46:8748–8758
46. Yu B, Yu Z, Qi P-P et al (2015) Discovery of orally active anticancer candidate CFI-400945 derived from biologically promising spirooxindoles: Success and challenges. Eur J Med Chem 95:35–40
47. Yeung BKS, Zou B, Rottmann M et al (2010) Spirotetrahydro β-Carbolines (Spiroindolones): a new class of potent and orally efficacious compounds for the treatment of malaria. J Med Chem 53:5155–5164
48. Rottmann M, McNamara C, Yeung BKS et al (2010) Spiroindolones, a potent compound class for the treatment of malaria. Science 329:1175–1180
49. White NJ, Pukrittayakamee S, Phyo AP et al (2014) Spiroindolone KAE609 for falciparum and vivax malaria. N Engl J Med 371:403–410
50. van Pelt-Koops JC, Pett HE, Graumans W et al (2012) The spiroindolone drug candidate NITD609 potently inhibits gametocytogenesis and blocks Plasmodium falciparum transmission to anopheles mosquito vector. Antimicrob Agents Chemother 56:3544–3548
51. Yu B, Qi P-P, Shi X-J et al (2014) Discovery of novel steroidal pyran–oxindole hybrids as cytotoxic agents. Steroids 88:44–52

52. Yu B, Shi X-J, Qi P-P et al (2014) Design, synthesis and biological evaluation of novel steroidal spiro-oxindoles as potent antiproliferative agents. J Steroid Biochem Mol Biol 141:121–134
53. Yu B, Yu D-Q, Liu H-M (2015) Spirooxindoles: promising scaffolds for anticancer agents. Eur J Med Chem 97:673–698
54. Yu B, Sun X-N, Shi X-J et al (2015) Efficient synthesis of novel antiproliferative steroidal spirooxindoles via the [3+2] cycloaddition reactions of azomethine ylides. Steroids 102: 92–100
55. Bin Y, Yi-Chao Z, Xiao-Jing S et al (2016) Natural product-derived spirooxindole fragments serve as privileged substructures for discovery of new anticancer agents. Anticancer Agents Med Chem 16:1315–1324
56. Zhang Y-L, Li Y-F, Wang J-W et al Multicomponent assembly of novel antiproliferative steroidal dihydropyridinyl spirooxindoles. Steroids 109:22–28
57. Shi X-J, Yu B, Wang J-W et al (2016) Structurally novel steroidal spirooxindole by241 potently inhibits tumor growth mainly through ROS-mediated mechanisms. Sci Rep 6:31607
58. Yu B, Xing H, Yu D-Q et al (2016) Catalytic asymmetric synthesis of biologically important 3-hydroxyoxindoles: an update. Beilstein J Org Chem 12:1000–1039
59. Aguilar A, Sun W, Liu L et al (2014) Design of chemically stable, potent, and efficacious MDM2 inhibitors that exploit the retro-mannich ring-opening-cyclization reaction mechanism in spiro-oxindoles. J Med Chem 57:10486–10498
60. Ding K, Lu Y, Nikolovska-Coleska Z et al (2005) Structure-based design of potent non-peptide MDM2 inhibitors. J Am Chem Soc 127:10130–10131
61. Smart BE (2001) Fluorine substituent effects (on bioactivity). J Fluor Chem 109:3–11
62. Ding K, Lu Y, Nikolovska-Coleska Z et al (2006) Structure-based design of spiro-oxindoles as potent, specific small-molecule inhibitors of the MDM2–p53 interaction. J Med Chem 49:3432–3435
63. Lin J, Chen J, Elenbaas B et al (1994) Several hydrophobic amino acids in the p53 amino-terminal domain are required for transcriptional activation, binding to MDM-2 and the adenovirus 5 E1B 55-kD protein. Genes Dev 8:1235–1246
64. Picksley SM, Vojtesek B, Sparks A et al (1994) Immunochemical analysis of the interaction of p53 with MDM2;–fine mapping of the MDM2 binding site on p53 using synthetic peptides. Oncogene 9:2523–2529
65. Shangary S, Qin D, McEachern D et al (2008) Temporal activation of p53 by a specific MDM2 inhibitor is selectively toxic to tumors and leads to complete tumor growth inhibition. Proc Natl Acad Sci USA 105:3933–3938
66. Zhao Y, Liu L, Sun W et al (2013) Diastereomeric spirooxindoles as highly potent and efficacious MDM2 inhibitors. J Am Chem Soc 135:7223–7234
67. Zhao Y, Yu S, Sun W et al (2013) A Potent small-molecule inhibitor of the MDM2–p53 interaction (MI-888) achieved complete and durable tumor regression in mice. J Med Chem 56:5553–5561
68. Shu L, Li Z, Gu C et al (2013) Synthesis of a spiroindolinone pyrrolidinecarboxamide MDM2 antagonist. Org Proc Res Dev 17:247–256
69. Hoffman-Luca CG, Yang C-Y, Lu J et al (2015) Significant differences in the development of acquired resistance to the MDM2 inhibitor SAR405838 between in vitro and in vivo drug treatment. PLoS ONE 10:e0128807
70. Hoffman-Luca CG, Ziazadeh D, McEachern D et al (2015) Elucidation of acquired resistance to Bcl-2 and MDM2 inhibitors in acute leukemia in vitro and in vivo. Clin Cancer Res 21:2558–2568
71. Carry J-C, Garcia-Echeverria C (2013) Inhibitors of the p53/hdm2 protein–protein interaction —path to the clinic. Bioorg Med Chem Lett 23:2480–2485
72. Miyazaki M, Setoguchi M, Sugimoto Y et al (2012) Dispiropyrrolidine derivative. EP20120755073
73. Wang S, Sun W, Aguilar A et al (2014) Spiro-oxindole MDM2 antagonists. US 14/485,054

74. Phelps D, Bondra K, Seum S et al (2015) Inhibition of MDM2 by RG7388 confers hypersensitivity to X-radiation in xenograft models of childhood sarcoma. Pediatr Blood Cancer 62:1345–1352
75. Zhang Z, Ding Q, Liu J-J et al (2014) Discovery of potent and selective spiroindolinone MDM2 inhibitor, RO8994, for cancer therapy. Bioorg Med Chem 22:4001–4009
76. Zhang Z, Chu X-J, Liu J-J et al (2013) Discovery of potent and orally active p53-MDM2 inhibitors RO5353 and RO2468 for potential clinical development. ACS Med Chem Lett 5:124–127
77. Luk KC, So SS, Zhang J et al (2006) Oxindole derivatives. PCT/EP2006/063475
78. Ding Q, Jiang N, Yang S et al (2009) Spiroindolinone derivatives. US 12/272,870
79. Ding Q, Liu JJ, Zhang Z (2007) Spiroindolinone derivatives. PCT/EP2007/052038
80. Liu JJ, Tilley JW, Zhang Z (2009) 3,3-spiroindolinone derivatives. CN 200880016425
81. Liu JJ, Tilley JW, Zhang Z (2010) 3,3-spiroindolinone derivatives as anticancer agents. PCT/EP2010/051757
82. Liu JJ, Zhang Z (2008) Spiroindolinone derivatives. PCT/EP2008/055831
83. Chu XJ, Ding Q, Jiang N *et al* (2012) Substituted Spiro[3H-Indole-3,6′(5′H)-[1H]Pyrrolo [1,2c]Imidazole-1′,2(1H,2′H)-diones. US 20120071499
84. Pfafferott G, Oberhammer H, Boggs JE et al (1985) Geometric structure and pseudorotational potential of pyrrolidine. An ab initio and electron diffraction study. J Am Chem Soc 107:2305–2309
85. Cremer D, Pople JA (1975) General definition of ring puckering coordinates. J Am Chem Soc 97:1354–1358
86. Madison V (1977) Flexibility of the pyrrolidine ring in proline peptides. Biopolymers 16:2671–2692
87. Ramachandran GN, Lakshminarayanan AV, Balasubramanian R et al (1970) Studies on the conformation of amino acids XII. Energy calculations on prolyl residue. Biochim Biophys Acta (BBA)—Protein Struct 221:165–181
88. DeTar DF, Luthra NP (1977) Conformations of proline. J Am Chem Soc 99:1232–1244
89. Bertamino A, Soprano M, Musella S et al (2013) Synthesis, in vitro, and in cell studies of a new series of [Indoline-3,2′-thiazolidine]-based p53 modulators. J Med Chem 56:5407–5421
90. Ivanenkov YA, Vasilevski SV, Beloglazkina EK et al (2015) Design, synthesis and biological evaluation of novel potent MDM2/p53 small-molecule inhibitors. Bioorg Med Chem Lett 25:404–409
91. Kumar A, Gupta G, Bishnoi AK et al (2015) Design and synthesis of new bioisosteres of spirooxindoles (MI-63/219) as anti-breast cancer agents. Bioorg Med Chem 23:839–848
92. Li Bo ZR, He Gu, Li Guo, Wei Huang (2013) Molecular docking, QSAR and molecular dynamics simulation on spiro-oxindoles as MDM2 inhibitors. Acta Chim Sinica 71: 1396–1403
93. Ribeiro CJA, Amaral JD, Rodrigues CMP et al (2014) Synthesis and evaluation of spiroisoxazoline oxindoles as anticancer agents. Bioorg Med Chem 22:577–584
94. Huang W, Cai L, Chen C et al (2015) Computational analysis of spiro-oxindole inhibitors of the MDM2-p53 interaction: insights and selection of novel inhibitors. J Biomol Struct Dyn 34:1–11
95. Zhou R, Wu Q, Guo M et al (2015) Organocatalytic cascade reaction for the asymmetric synthesis of novel chroman-fused spirooxindoles that potently inhibit cancer cell proliferation. Chem Commun 51:13113–13116
96. Wang S, Jiang Y, Wu S et al (2016) Meeting organocatalysis with drug discovery: asymmetric synthesis of 3,3′-Spirooxindoles fused with tetrahydrothiopyrans as novel p53-MDM2 inhibitors. Org Lett 18:1028–1031
97. Patil SP (2013) FOLICation: engineering approved drugs as potential p53–MDM2 interaction inhibitors for cancer therapy. Med Hypotheses 81:1104–1107